ELSEVIER

Chemical Engineering Journal 80 (2000) 105–117

Chemical Engineering Journal

www.elsevier.com/locate/cej

Applications of the phenomenological theory to several published experimental cases of sedimentation processes

R. Bürger [a,*], F. Concha [b], F.M. Tiller [c]

[a] *Institute of Mathematics A, University of Stuttgart, Pfaffenwaldring 57, D-70569 Stuttgart, Germany*
[b] *Departamento de Ingeniería Metalúrgica, Universidad de Concepción, Casilla 53-C, Correo 3, Concepción, Chile*
[c] *Chemical Engineering Department, University of Houston, Houston, TX 77204-4792, USA*

Abstract

In one space dimension, the phenomenological theory of sedimentation predicts the sedimentation–consolidation behavior of a flocculated suspension in dependence of two constitutive functions describing its material behavior, the solids flux density (or hindered settling function) and the solid effective stress. These functions are assumed to depend only on the local volumetric solids concentration. In this contribution, we review several experimental and theoretical studies of sedimentation in settling columns. We first resume the theories that have been employed to interpret the experimental measurements and then apply the phenomenological model to the available data. The two constitutive functions involved are determined from the published concentration, permeability and effective stress data. The mathematical model is then solved numerically using these functions, and the resulting predictions of settling behavior are compared with the respective authors' experimental findings and interpretations. In one case, the information obtained from a batch settling experiment is used to simulate continuous sedimentation.

Keywords: Batch sedimentation; Flocculated suspension; Settling column; Numerical simulation; Phenomenological theory

1. Introduction

Batch settling is probably the simplest way to separate a flocculated suspension into a concentrated sediment and a clear liquid. Experimental and theoretical studies of this process have been published for almost a century now, starting with the works by Nichols in 1908 [1], Mishler in 1912 [2] and Coe and Clevenger in 1916 [3], but it was only in the last 20 years that a rigorous phenomenological theory has evolved which provides a clear understanding of the phenomena occurring during the sedimentation in settling columns and in continuous thickeners. This theory is based on the theory of mixtures and models a suspension as a mixture of two superimposed continuous media. The modelling from the mass and linear momentum balances of the components. The introduction of kinematic and dynamic constitutive assumptions and a subsequent dimensional analysis lead in one space dimension to a scalar hyperbolic–parabolic field equation for the solids volumetric concentration, together with an algebraic relationship for the excess pore pressure gradient. The first author's contribution to this issue [4] presents this theory in detail, hence it is outlined very briefly in this paper (see Section 2).

The material behavior of the suspension is described by two constitutive functions, the Kynch batch flux density function f_{bk} and the effective solid stress, σ_{e}, which are assumed to depend on the local volumetric solids concentration ϕ only and have to be given explicitly on the entire interval of concentration values from zero to the maximum concentration. Once these functions and initial and boundary conditions are given, the field equation can be solved numerically to predict the sedimentation behavior of the suspension.

The authors have published several studies of simulated hypothetical behavior of flocculated suspensions in batch or continuous ideal thickeners [5–7]. It is the purpose of this paper to employ published experimental concentration, excess pore pressure and effective solid stress data to determine the functions $f_{\mathrm{bk}}(\phi)$ and $\sigma_{\mathrm{e}}(\phi)$ for each experimental case, and to use this information to simulate the respective experiment. The numerical solution is then compared with the experimentally observed batch settling behavior. In Section 3, we present these results.

To demonstrate that the phenomenological theory and the numerical algorithm are not limited to batch sedimentation but also apply to the continuous case, we consider the study of the dynamic behavior of a continuous thickener by

* Corresponding author. Tel.: +49-711-6857647; fax: +49-711-6855599.
E-mail addresses: buerger@mathematik.uni-stuttgart.de (R. Bürger), fconcha@udec.cl (F. Concha).

1383-5866/00/$ – see front matter
PII: S1383-5866(00)00090-3

Nomenclature

Latin symbols

a	particle diameter in Eq. (20)
$a(\phi)$	diffusion coefficient
C	prameter in the Kynch batch flux density function
e	void ratio
$f_{\mathrm{bk}}\ (\phi)$	Kynch batch flux density function
$f^i_{\mathrm{bk}}(\phi)$, $i = 1, \ldots, 6$	functions $f_{\mathrm{bk}}\ (\phi)$ in different test cases
f_{F}	feed flux
f^1_{F}, f^2_{F}	steady state values of f_{F} (see Table 2)
g	acceleration due to gravity
k_{f}	permeability given by Eq. (22)
K	permeability
K_0	permeability under zero effective stress
K^{BS}	permeability in the sense of Been and Sills [30]
L	feeding level height
n	parameter in Eq. (19)
p_a	parameter in Eqs. (13) and (14)
p_{e}	excess pore pressure
p_s, p_{f}	solid/fluid component phase pressures
q	volume average velocity
t	time
v_{s}, v_{f}	solid/fluid phase velocities
v_{r}	drift velocity
u_∞	parameter in the Kynch batch flux density function
$\tilde{u}_\infty$	parameter in Eq. (20)
z	height

Greek symbols

$\alpha(\phi)$	resistance coefficient
β	parameter in Eq. (13)
δ	parameter in Eq. (14)
Δz	spatial discretization parameter
$\Delta\varrho$	solid–fluid mass density difference
$\overline{\Delta\varrho}$	intermediate density difference
ϕ	volumetric solids concentration
ϕ_{c}	critical concentration
ϕ^i_{c}, $i = 1, 2, 3, 5, 6$	values of ϕ_{c} used in different test cases
ϕ^1_{D}, ϕ^2_{D}	steady state discharge concentration values see Table 2
$\phi_L(t)$	concentration prescribed at $z = L$
ϕ^1_{L}, ϕ^2_{L}	steady state values of ϕ_L, see Table 2
$\phi_{\max}$	maximum concentration
μ_{f}	dynamic viscosity of the pure fluid
ν_{f}	kinematic viscosity of the pure fluid
$\varrho(\phi)$	local density of the mixture
ϱ_{s}, ϱ_{f}	solid/fluid mass densities
$\sigma_{\mathrm{e}0}$	parameter in Eq. (19)
$\sigma_{\mathrm{e}}(\phi)$	effective solid stress function
$\sigma^i_{\mathrm{e}}(\phi)$, $i = 1, 2, 3, 5, 6$	functions $\sigma_{\mathrm{e}}(\phi)$ in different test cases

Damasceno et al. [8]. These authors used effective stress and permeability data from a batch settling test for the simulation of continuous thickening. However, their mathematical approach is slightly different from ours. In Section 4, we recalculate their example. Conclusions which can be drawn from our case study are collected in Section 5.

2. The mathematical model

Consider the settling of a flocculated suspension under the idealizing assumptions stated in [4,7]. Here, we may neglect the effect of viscosity, as justified in a one-dimensional framework [9–11], and the advective acceleration terms, since the Froude number of the systems considered here is small (see [4]). Furthermore, as is shown in [12], the component phase pressures p_{f} and p_{s}, which are theoretical variables, may be replaced by the excess pore pressure p_{e} and the effective solid stress σ_{e}, which are measurable quantities, by equations stated explicitly in [4].

The effective solid stress, σ_{e}, is assumed to be given as a constitutive function. We assume that σ_{e} is constant while the solid particles are in hindered settling, i.e. while their volumetric concentration has not yet reached a critical concentration or gel point ϕ_{c}, and that it is a monotonically increasing function for $\phi > \phi_{\mathrm{c}}$; consequently, we have

$$\sigma'_{\mathrm{e}}(\phi) = \frac{\mathrm{d}\sigma_{\mathrm{e}}}{\mathrm{d}\phi} \begin{cases} = 0 & \text{for } \phi \le \phi_{\mathrm{c}}; \\ > 0 & \text{for } \phi > \phi_{\mathrm{c}}. \end{cases} \tag{1}$$

Under certain additional constitutive assumptions, the following set of equations can be derived from the solid and liquid component mass and linear momentum balances (see [4,13]):

$$\frac{\partial\phi}{\partial t} + \frac{\partial(\phi v_{\mathrm{s}})}{\partial z} = 0, \tag{2}$$

$$q = q(t), \tag{3}$$

$$\frac{\partial\sigma_{\mathrm{e}}}{\partial z} = -\Delta\varrho\phi g - \frac{\alpha(\phi)}{1-\phi}\, v_{\mathrm{r}}, \tag{4}$$

$$\frac{\partial p_{\mathrm{e}}}{\partial z} = \frac{\alpha(\phi)}{1-\phi}\, v_{\mathrm{r}}, \tag{5}$$

where t is time, z the height variable, v_{s} the solid phase velocity, $q = \phi v_{\mathrm{s}} + (1-\phi)v_{\mathrm{f}}$ the volume average velocity, $\Delta\varrho = \varrho_{\mathrm{s}} - \varrho_{\mathrm{f}}$ where ϱ_{s} and ϱ_{f} are the solid and liquid mass densities, g the acceleration due to gravity, $\alpha(\phi)$ the resistance coefficient which has to be given as a constitutive function, and v_{r} is the solid–liquid relative velocity or drift

velocity. Using the Kynch batch flux density function $f_{\mathrm{bk}}(\phi)$ given by

$$f_{\mathrm{bk}}(\phi) = -\frac{\Delta\varrho g\phi^2(1-\phi)^2}{\alpha(\phi)}, \tag{6}$$

we obtain from Eq. (4)

$$\phi(1-\phi)v_{\mathrm{r}} = f_{\mathrm{bk}}(\phi)\left(1+\frac{\sigma_{\mathrm{e}}'(\phi)}{\Delta\varrho g\phi}\,\frac{\partial\phi}{\partial z}\right). \tag{7}$$

Using the definition of q, it is easy to see that

$$\phi v_{\mathrm{s}} = q\phi + \phi(1-\phi)v_{\mathrm{r}}. \tag{8}$$

Thus, in view of (Eq. (7)), Eq. (3) can be rewritten as

$$\frac{\partial\phi}{\partial t} + \frac{\partial}{\partial z}\left(q\phi + f_{\mathrm{bk}}(\phi)\left(1+\frac{\sigma_{\mathrm{e}}'(\phi)}{\Delta\varrho g\phi}\,\frac{\partial\phi}{\partial z}\right)\right),$$

or as

$$\frac{\partial\phi}{\partial t} + \frac{\partial}{\partial z}\left(q(t)\phi + f_{\mathrm{bk}}(\phi)\right) = \frac{\partial}{\partial z}\left(a(\phi)\frac{\partial\phi}{\partial z}\right), \tag{9}$$

where the diffusion coefficient $a(\phi)$ is defined by

$$a(\phi) = -\frac{f_{\mathrm{bk}}(\phi)\sigma_{\mathrm{e}}'(\phi)}{\Delta\varrho g\phi}.$$

Finally, inserting Eqs. (6) and (7) into Eq. (5) yields

$$\frac{\partial p_{\mathrm{e}}}{\partial z} = -\Delta\varrho g\phi - \sigma_{\mathrm{e}}'(\phi)\frac{\partial\phi}{\partial z}. \tag{10}$$

Eqs. (9) and (10) form now the field equations from which ϕ and p_{e} are determined (see [4]). The function f_{bk}, which is in most cases prescribed instead of $\alpha(\phi)$, should satisfy the conditions

$$\begin{aligned} &f_{\mathrm{bk}}(0) = f_{\mathrm{bk}}(\phi_{\max}) = 0,\\ &f_{\mathrm{bk}}(\phi) < 0 \quad \text{for} \quad 0 < \phi < \phi_{\max}, \qquad f_{\mathrm{bk}}'(0) < 0,\\ &f_{\mathrm{bk}}'(\phi_{\max}) > 0 \end{aligned} \tag{11}$$

stated by Kynch [15], where $\phi_{\max}$ is the maximum concentration. The last condition ensures that batch settling processes of ideal suspensions, for which $\sigma_{\mathrm{e}} \equiv 0$ is assumed, terminate within finite time. However, in practice and for flocculated suspensions for which σ_{e}, does not vanish, empirical approaches such as Michael and Bolger's [16] generalization

$$\begin{aligned} f_{\mathrm{bk}}(\phi) = u_\infty\phi\left(1-\frac{\phi}{\phi_{\max}}\right)^C, \quad u_\infty < 0,\\ 0 < \phi_{\max} \le 1, \quad C > 1 \end{aligned} \tag{12}$$

of Richardson and Zaki's equation [17] are employed, for which $f_{\mathrm{bk}}'(\phi_{\max}) = 0$ holds. The constants u_∞ and C have to be determined experimentally.

Eq. (9) is a second-order scalar parabolic equation, which degenerates for $\phi \le \phi_{\mathrm{c}}$, into the first-order hyperbolic equation of Kynch's theory and its extensions to continuous thickening. In the context of batch sedimentation, the type-change interface, where $\phi = \phi_{\mathrm{c}}$ is valid, separates the hindered settling zone from the compression zone. Its location is in general unknown a priori, which requires special treatments for the mathematical analysis and for the numerical solution, see the contribution by Bürger et al. to this issue, [13] and chapter 9 of [18] for details. Eq. (10) permits the calculation of the excess pore pressure a posteriori from the concentration distribution.

Eqs. (9) and (10) are considered in an ideal continuous thickener (ICT, see [19,20] and Fig. 1 in [18]) of feeding level height L. In this simple set-up, the continuous feed is modeled by a boundary condition at $z = L$. For example, we might prescribe the concentration $\phi(z = L, t) = \phi_L(t)$ for $t > 0$, where $\phi_L(t)$ is a given function, although in a mathematically rigorous sense, this boundary condition should be reformulated as a set-valued entropy boundary condition [14].

The volume average velocity $q(t) \le 0$ can be described by discharge control; setting $q \equiv 0$ corresponds to a settling column. This condition is equivalent to prescribing that the total solids volume flux through $z = 0$ reduces to its convective part, i.e. $v_{\mathrm{s}} = q(t)$, which can be rewritten as the boundary condition

$$f_{\mathrm{bk}}(\phi) - a(\phi)\left.\frac{\partial\phi}{\partial z}\right|_{z=0} = 0, \quad t > 0.$$

Again, a mathematically strict treatment would require that we rewrite this condition in a slightly different way (see [14]).

The field equation (Eq. (9)) together with these initial and boundary conditions was solved by the finite difference operator splitting method outlined in [18], see [13] for a detailed description. The spatial resolution was $\Delta z = L/400$ in Figs. 3, 4, 9 and 10; $\Delta z = L/2000$ in Figs. 5 and 6; $\Delta z = L/1000$ in Figs. 7 and 8; and $\Delta z = L/800$ in Figs. 11 and 12.

3. Comparison with published batch settling experiments

We selected four different published studies of batch sedimentation of flocculated slurries. Table 1 gives an overview of the experiments, while Fig. 1 presents plots of the functions $f_{\mathrm{bk}}(\phi)$ and $\sigma_{\mathrm{e}}(\phi)$ used in the simulations. These functions are given explicitly below.

3.1. Comparison with CATSCAN measurements of the settling of a flocculated kaolin suspension

The study starts considering computerized axial tomographic scanner (CATSCAN) concentration profile measurements performed by Tiller et al. [21,22]. In addition, the solids pressure, corresponding to the effective solid stress in this paper, was measured at the bottom of the vessel. Tiller

Table 1
Overview of the experimental data

Authors	Materials	Methods	L (m)	$\Delta\varrho$ (kg/m^3)	ϕ_0
Tiller et al., 1992 [21,22]	Kaolin Flat D/water	CATSCAN	0.16	1562.0	0.05
Bergström, 1992 [27]	Alumina/decalin	γ-ray absorption	0.198	3083.0	0.15
Been and Sills [30], experiment 11	Estuarine mud/water	X-ray/transducers	1.802	1689.7	0.02954
Been and Sills [30], experiment 15	Estuarine mud/water	X-ray/transducers	0.643	1536.1	0.09231
Dreher, 1997 [34]	Kaolin/water	γ-ray/standpipes	1.19	1560.0[a]	0.07
Damasceno et al., 1992 [8]	Calcium carbonate/water	γ-ray/absorption	2.00[b]	1660.0	0.0[b]

[a]Estimated.
[b]Used in this paper.

and Leu [23] correlated the local solidosity, or solids volume fraction, ϕ, and the local permeability, K, to the effective solid stress by the formulas (in our notation)

$$\phi = \phi_c \left(1 + \frac{\sigma_e}{p_a}\right)^{\beta}, \tag{13}$$

$$K = K_0 \left(1 + \frac{\sigma_e}{p_a}\right)^{-\delta}, \tag{14}$$

where β, δ and p_a are parameters and K_0 is the permeability under zero effective stress, i.e. is at the sediment surface, see Eqs. (8) and (9) in [24]. It should be noted that these

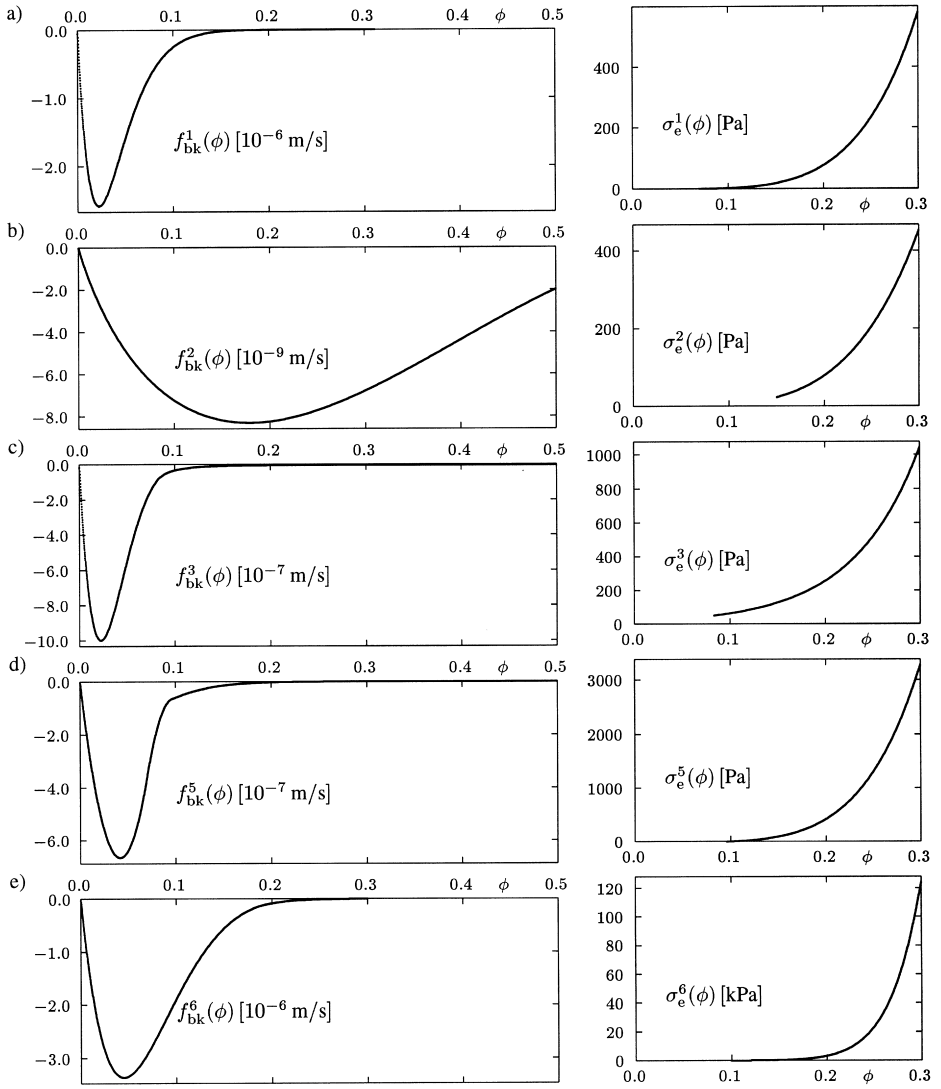

Fig. 1. Kynch batch flux density and effective solid stress functions $f_{bk}(\phi)$ and $\sigma_e(\phi)$ determined from data published by (a) Tiller et al. [22]; (b) Bergström [27]; (c) Been and Sills [30]; (d) Dreher [34]; and (e) Damasceno et al. [8].

equations are only valid in the compression zone. The local permeability appears in the modified Darcy equation (Eq. (10) in [25]), which can be written here as

$$\frac{\partial \sigma_e}{\partial z} = -\Delta\varrho g\phi - \frac{\mu_f(1-\phi)v_r}{K} \tag{15}$$

(see Eq. (58) in [26]), where μ_f is the dynamic viscosity of the pure liquid. Assuming $K = K(\phi)$, comparing the right-hand parts of Eqs. (4) and (15) and using the definition of $f_{bk}(\phi)$ yields

$$f_{bk}(\phi) = -\frac{K(\phi)\Delta\varrho g\phi^2}{\mu_f}. \tag{16}$$

This formula permits the determination of the Kynch batch flux density function for the compression zone, identified with the region where $\phi > \phi_c$ is valid, from permeability data. Of course, one could also employ the equivalent formula

$$\alpha(\phi) = \frac{\mu_f(1-\phi)^2}{K(\phi)}$$

for the determination of the resistance coefficient $\alpha(\phi)$ from permeability data.

To obtain constitutive equations for the kaolin used in the experiments, first an almost stationary concentration profile, measured after 2 days, was considered [21]. After that time, the sediment is almost at equilibrium and there is no solid–liquid relative motion, i.e. it may be assumed that v_r has vanished. Under that condition, Eqs. (4) and (15) reduce to

$$\frac{\partial \sigma_e}{\partial z} = -\Delta\varrho g\phi. \tag{17}$$

If the critical concentration ϕ_c is known or chosen appropriately and attained at a height z_c denoting the sediment level, then we may assume that $\sigma_e = 0$ for $z \geq z_c$. Integrating Eq. (17) downwards with respect to z, using the measured stationary concentration profile, will yield data to which an empirical approach for $\sigma_e = \sigma_e(\phi)$ can be fitted.

Tiller and Kwon [21] compared various choices of ϕ_c and the corresponding predictions of the maximum effective solid stress value at the bottom of the settling column with the measured value, and concluded that $\phi_c = \phi_c^1 = 0.07$ was the best choice for the kaolin suspension. Choosing $p_a = 0.04$ Pa, the exponent $\beta = 0.2$ was obtained in Eq. (13); this yields the effective solid stress equation $\sigma_e = 0$ for $\phi \leq \phi_c^1$ and

$$\sigma_e(\phi) = \sigma_e^1(\phi) = p_a\left[\left(\frac{\phi}{\phi_c^1}\right)^{1/\beta} - 1\right]$$

$$= 0.4\left[\left(\frac{\phi}{0.07}\right)^5 - 1\right] \text{ Pa} \quad \text{for } \phi > \phi_c^1. \tag{18}$$

By a similar method of data fitting, using concentration profiles obtained after 2000 and 3000 s and again taking the maximum measured effective solid stress into account, Tiller and Kwon [21] obtained the parameters $K_0 = 1.26 \times 10^{-11}$ m^2 and $\delta = 1.24$, leading via Eq. (18) to

$$K(\phi) = 8.709 \times 10^{-19}\phi^{-6.2}\,\text{m}^2.$$

This expression could be inserted into Eq. (16) to obtain an explicit representation of f_{bk} in the compression zone, i.e. for $\phi > \phi_c$, which could be combined with a second formula for $0 \leq \phi \leq \phi_c$, the hindered settling zone. This methodology has been adopted in some of the next examples. However, since the permeability values have not been measured and represent only estimates, we can also use these values as raw data, transform them to values of $f_{bk}(\phi)$, and approximate this set of discrete points by some semi-empirical function. We choose an approach of Michaels and Bolger's type (Eq. (12)) and require that

$$\frac{f_{bk}(0.05)}{0.05} = -3.2 \times 10^{-4}\,\text{m/s},$$

which is the observed falling velocity of the clear liquid–suspension interface, or settling rate, according to the Rankine–Hugoniot jump condition. The final flux density function is

$$f_{bk}(\phi) = f_{bk}^1(\phi) = -3.082736 \times 10^{-4}\phi(1-2\phi)^{21.5}\,\text{m/s},$$
$$0 \leq \phi \leq \phi_{max} = 0.5,$$

see Fig. 1a and Fig. 2.

Fig. 3 shows the measured concentration profiles compared to our numerical simulation.

3.2. Comparison with γ-ray measurements of a flocculated alumina suspension

Bergström [27] presented an interesting study of settling experiments with alumina suspensions. His main objective was the investigation of the effect of interparticle energy on the settling process. Therefore, he added to the mixture fatty acids of five different hydrocarbon chain lengths, which are adsorbed at the solid–liquid interface. The lengths of the adsorbed fatty acid molecules determine the distance of

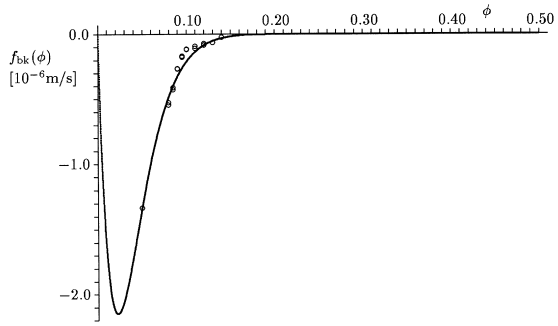

Fig. 2. Batch flux density function determined from permeability calculations and the clear liquid/suspension interface falling velocity.

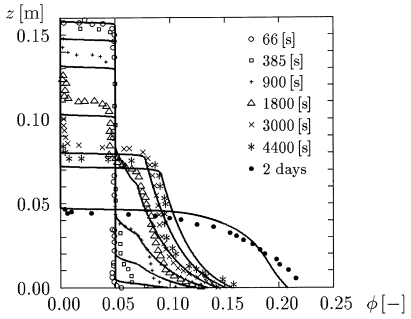

Fig. 3. CATSCAN concentration profile measurements by Tiller et al. [22] compared with numerical simulation.

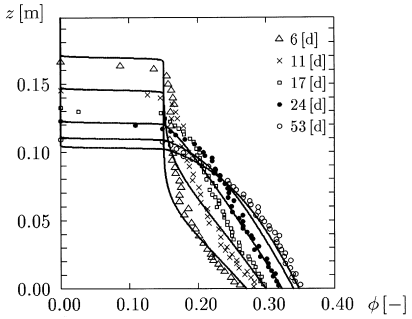

Fig. 4. γ-Ray concentration profile measurements compared with numerical simulation of the corresponding phenomenological sedimentation model.

closest approach and thus the interaction energy at contact (see [27]). It was found that an initial concentration of 0.10 would still produce a free-settling zone, therefore initial concentrations of roughly 0.15, assumed to be the critical one, were chosen. The absorption by γ-rays led to experimental concentration profiles, and the effective solid stress in a given height was determined in the same way as in the previous example, namely, by integrating Eq. (17) using an equilibrium concentration profile. Bergström [27] showed that the stress curves could be fitted to a power law,

$$\sigma_e(\phi) = \sigma_e^2(\phi) = \sigma_{e0}\phi^n \quad \text{for } \phi > \phi_c^2 = 0.15. \tag{19}$$

Here, we select the 'intermediate' example of the addition of heptanoic acid, for which Bergström [27] found the exponent $n = 4.3$ to be suitable; his plot suggests taking $\sigma_{e0} = 80\ 000$ Pa. Following Auzerais et al. [28], he suggests employing Brinkman's permeability formula [29] modelling the porous medium as a single sphere embedded in an effective medium, which is, in our mathematical framework, equivalent to

$$f_{bk}(\phi) = f_{bk}^2(\phi) = \widetilde{u_\infty}\,\frac{\phi(2-3\phi)^2}{3\phi + 4 + 3(8\phi - 3\phi^2)^{1/2}},$$
$$\widetilde{u_\infty} = -\frac{2a^2\Delta\varrho}{9\mu_f}, \tag{20}$$

where a is an average particle radius. Using the data provided by Bergström [27], namely the (very small) particle diameter $a = 2\times10^{-7}$ m, the densities $\varrho_s = 3.96$ and $\varrho_f = 0.877\ \mathrm{kg/m^3}$ (we neglect here the small amount of fatty acid) and $\mu_f = 0.0026$ Pa s, we obtain $\widetilde{u_\infty} = -1.034\times10^{-7}$ m/s. Inserting these parameters and $\phi_0 = 0.15$ into the formula for the initial settling rate given by Auzerais et al. [28], however, showed that the value of $\widetilde{u_\infty}$, was too small in modulus to describe the observed behavior. We amended this by replacing this value with $u_\infty = -1.737\times10^{-7}$ m/s. Note that formula (Eq. (20)) is well defined also for $0 \le \phi \le \phi_c$. Since no information on preliminary experiments with more dilute suspensions of sub-critical initial concentrations was published, which would have allowed fixing values of $f_{bk}(\phi)$ by using settling rate measurements as in the previous experiment, we decided to employ Eq. (20) with u_∞, instead of $\widetilde{u_\infty}$ for the whole range of concentration values. The functions $f_{bk}^2(\phi)$ and $\sigma_e^2(\phi)$ are plotted in Fig. 1b, and the numerical result is presented in Fig. 4.

3.3. Comparison with X-ray concentration and excess pore pressure measurements of estuarine mud slurries

The paper by Been and Sills [30] is one of the classical studies of the settling of flocculated suspensions and has been cited by many authors. Been and Sills performed experiments in settling columns using slurries of water mixed with real estuarine mud, producing various initial densities. They also published the mass of soil, here identified with the dry solid phase, and the initial height of the mixture such that the effective solid–liquid mass density difference and the initial solids volume fraction could be calculated. This shows that the solid material, as a real soil, was slightly different in each experiment.

Been and Sills measured the excess pore pressure by transducers or standpipes. The advantage of having excess pore pressure data available is obvious, since then Eq. (5) instead of Eq. (17) may be used to derive a constitutive relationship for σ_e, i.e. it is not necessary to wait until steady state is reached, in which the excess pore pressure has vanished. Although the effective solid stress data, presented graphically by Been and Sills ([30], Figs. 13 and 16), do not support the concept of choosing one unique set of parameters for all experiments, we found that qualitative agreement of the simulations with the measurements could be attained by approximating their data by setting $\phi_c = \phi_c^3 = 1/12 = 0.083$, $\sigma_e(\phi) = \sigma_e^3(\phi) = 0$ for $\phi \le \phi_c^3$ and

$$\sigma_e(\phi) = \sigma_e^3(\phi) = 15.56\exp(14.01\phi)\ \text{Pa} \quad \text{for } \phi > \phi_c^3.$$

A similar exponential fit was employed by Becker [31]. The permeability was not measured directly. However, once a constitutive equation for σ_e is chosen, estimates of the solids phase velocity v_s may be used to obtain values of $K(\phi)$ from Eq. (15). These estimates follow from the 'Lagrangian paths' [22] (see also [32,33]) of given sets of particles, which can be constructed from the succession of concentration profiles. For their experiments 10–15, Been and Sills plotted the

permeability data, in a logarithmic scale, against the void ratio $e = (1-\phi)/\phi$. Their definition of permeability, denoted here by K^{BS}, is related to $K(\phi)$ by $K^{\mathrm{BS}} = K(\phi)g/\nu_{\mathrm{f}}$, where ν_{f} is the kinematic viscosity of the liquid. For simplicity, we approximate their cloud of data by a straight line, obtaining

$$K^{\mathrm{BS}}(\phi) = 8.4822 \times 10^{-9} \exp\left(\frac{0.6168(1-\phi)}{\phi}\right) \mathrm{m/s}.$$

In view of formula (Eq. (16)), we obtain

$$f_{\mathrm{bk}}(\phi) = -\frac{\Delta\varrho\phi^2 K^{\mathrm{BS}}(\phi)}{\varrho_{\mathrm{f}}} \quad \text{for } \phi > \phi_{\mathrm{c}}^3, \tag{21}$$

where different values of $\Delta\varrho$ have to be used for each experiment.

To show that the phenomenological model predicts the observed settling behavior correctly, we consider their experiments 11 and 15, for which both experimental density and excess pore pressure profiles have been published (see Figs. 5–8 in [30]). The decisive difference between these experiments is the initial concentration: in experiment 11, the initial suspension was so dilute that effective solid stress did not exist initially and that a distinctive hindered settling zone could form, while the initial concentration in experiment 15 was so high that the solid particles did already form a network, i.e. the suspension was already in compression when the experiment started.

Been and Sills' experiment 7, for which the density measurements have also been plotted as a settling plot (see [30], Figs. 2 and 3) but for which the pressure measurements are available for one single time only (Fig. 4 in [30]), has already been simulated by Bürger et al. [5,7].

Using the density differences given in Table 1, we obtain

$$f_{\mathrm{bk}}(\phi) = f_{\mathrm{bk}}^3(\phi) = -1.433 \times 10^{-8}\phi^2 \exp \times \left(\frac{0.6168(1-\phi)}{\phi}\right) \mathrm{m/s} \quad \text{for } \phi > \phi_{\mathrm{c}}^3$$

for experiment 11 and

$$f_{\mathrm{bk}}(\phi) = f_{\mathrm{bk}}^4(\phi) = -1.303 \times 10^{-8}\phi^2 \exp \times \left(\frac{0.6168(1-\phi)}{\phi}\right) \mathrm{m/s} \quad \text{for } \phi > \phi_{\mathrm{c}}^3$$

for experiment 15. These flux density functions were cut at their local maximum 0.3084, which identifies this value with the maximum solids concentration. For $0 \le \phi \le \phi_{\mathrm{c}}^3$, we again consider Michael and Bolger's approach (Eq. (12)) and set $\overline{\Delta\varrho} = 1612.9\,\mathrm{kg/m^3}$. The parameters u_∞, $\phi_{\max}$ (not to be confused with 0.3084) and C were determined in such a way that the settling rate observed in experiment 11 coincided with the Rankine–Hugoniot condition, i.e. such that

$$\frac{f_{\mathrm{bk}}(0.02954)}{0.02954} = -2.93 \times 10^{-8}\,\mathrm{m/s}$$

is valid; that the inflection point is 0.045; and that the value of f_{bk} given by inserting ϕ_{c}^3 into formula (Eq. (12)) coincides

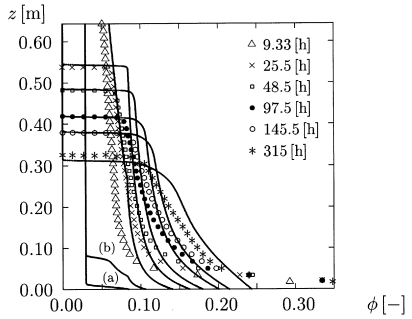

Fig. 5. Comparison of X-ray concentration measurements of an estuarine slurry ([30], experiment 11) with numerical simulation of the phenomenological model. The symbols represent the experimental data. In addition, the simulated concentration profiles for $t = 7\,\mathrm{min}$ (a) and $t = 1\,\mathrm{h}$ (b) are shown.

with the value obtained from Eq. (21) using the intermediate density difference $\overline{\Delta\varrho}$. The estimate of the inflection point was inferred from the shape of the measured concentration profile at $t = 9.33\,\mathrm{h}$. Multiplying the resulting flux density function with the respective factors 1689.7/1612.9 and 1536.1/1612.9, we finally obtain the expressions

$$f_{\mathrm{bk}}^3(\phi) = -1.211 \times 10^{-4}\phi(1-7.226\phi)^{5.15}\,\mathrm{m/s} \quad \text{for } 0 \le \phi \le \phi_{\mathrm{c}}^3,$$

$$f_{\mathrm{bk}}^4(\phi) = -1.101 \times 10^{-4}\phi(1-7.226\phi)^{5.15}\,\mathrm{m/s} \quad \text{for } 0 \le \phi \le \phi_{\mathrm{c}}^3.$$

The functions $f_{\mathrm{bk}}^3(\phi)$ and $\sigma_{\mathrm{e}}^3(\phi)$ are plotted in Fig. 1c. Figs. 5 and 6 show our numerical simulations compared with Been and Sills' concentration and excess pore pressure data for experiment 11, while Figs. 7 and 8 show the analogous results for experiment 15.

Note that the initial height of the suspension was much higher in experiment 11 (see Table 1) than in experiment 15, and that we plotted only that part of the numerical results which made comparison with experiment 15 possible. Furthermore, Been and Sills presented their concentration measurements as solid lines ([30], Figs. 5 and 6). It may be assumed that these lines had been obtained by smooth

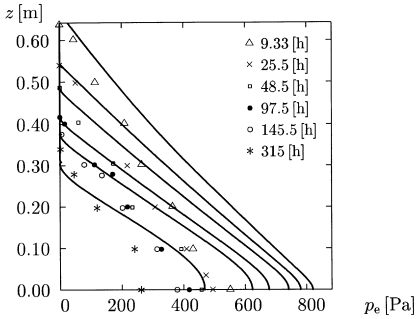

Fig. 6. Comparison of excess pore pressure measurements of an estuarine slurry ([30], experiment 11) with numerical simulation of the phenomenological model. The symbols represent the experimental data.

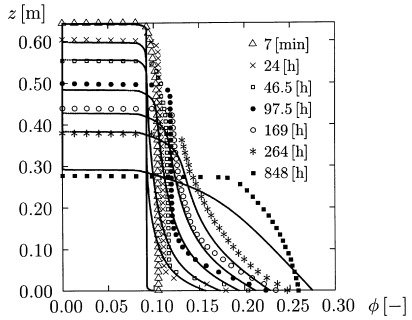

Fig. 7. Comparison of X-ray concentration measurements of an estuarine slurry ([30], experiment 15) with numerical simulation of the phenomenological model. The concentration profiles plotted in symbols represent the experimental data.

approximation of raw data, which they unfortunately did not show. To make distinction between the measured concentration profiles possible, we redrew each profile using different symbols for different times. It should also be mentioned that Been and Sills used a logarithmic scale for the mixture density, which we transformed into values of ϕ by linear approximation between integer values of $\varrho(\phi)g = (\phi\varrho_s + (1-\phi)\varrho_f)g$, measured in kN/m^3.

3.4. Comparison with γ-ray concentration and excess pore pressure measurements of a suspension of kaolin in water

Recently, Dreher [34] presented a study of batch settling of a flocculated kaolin suspension. In addition to concentration profiles obtained by γ-ray absorption, he also measured the excess pore pressure by ten equidistant standpipes.

In [34], transient effective solid stress data were obtained in the same way as by Been and Sills [30], which are plotted against the mixture density. Assuming that the dry material is of density $\varrho_s = 1560\,\mathrm{kg/m^3}$ as in other kaolin experiments (unfortunately, this value is not stated explicitly), we conclude from Dreher's observation that $\varrho = 1150\,\mathrm{kg/m^3}$ is the critical density, at which the effective stress begins to increase, that $\phi_c = \phi_c^5 = 0.096$ should be chosen. The experimental data could roughly be approximated by a power law similar to Eq. (18):

$$\sigma_e(\phi) = \sigma_e^5(\phi) = 11\left[\left(\frac{\phi}{\phi_c^5}\right)^5 - 1\right]\ \text{Pa for}\ \phi > \phi_c^5. \quad (22)$$

Again following Been and Sills [30], estimates of the permeability were obtained in [34] from the measured concentration profiles. The plot of the resulting values of the quantity k_f, in our notation given by

$$k_f = \frac{(1-\phi)K(\phi)\varrho_f g}{\mu_f}$$

and also referred to as permeability, against the local density $\varrho(\phi)$ using a logarithmic scale could be roughly approximated by a straight line. Using formula (16), this leads to

$$f_{bk}(\phi) = f_{bk}^5(\phi) = -4.877\times 10^{-4} \times \frac{\phi^2\exp(-45.078\phi)}{1-\phi}\ \mathrm{m/s}\quad \text{for}\ \phi > \phi_c^5. \quad (23)$$

The only experimental information available on f_{bk} for $0 < \phi \le \phi_c^5$ could be obtained from estimating the settling rate, leading to the requirement

$$f_{bk}^5(0.07) = -3.632\times 10^{-7}\ \mathrm{m/s}. \quad (24)$$

We decided to determine f_{bk}^5 as the unique second-order polynomial defined on [0.07, 0.096] which satisfies Eq. (24) and connects smoothly with the segment of f_{bk}^5 given by Eq. (23). Similarly, we determined another second-order polynomial defined on [0, 0.07] vanishing at ϕ=0 and connecting smoothly with the first, resulting in

$$f_{bk}^5(\phi) = \{(3.7942\,\phi^2 - 0.3175\phi)\times 10^{-4}\,\mathrm{m/s} \quad \text{for}\ 0 \le \phi \le 0.07,\ (-3.8178\phi^2 + 0.7482\phi - 0.0373)\times 10^{-4}\,\mathrm{m/s} \quad \text{for}\ 0.07 < \phi \le \phi_c^5$$

The functions $f_{bk}^5(\phi)$ and $\sigma_e^5(\phi)$ are given in Fig. 1d, while Fig. 9 shows the concentration measurements together with our simulation (in this case, we preferred to provide separate plots for each time, since the measured concentration data were rather scattered). The measurements and our calculation of p_e are collected in Fig. 10.

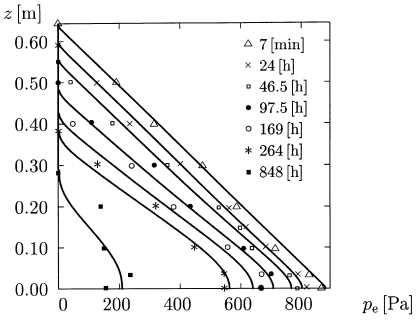

Fig. 8. Comparison of excess pore pressure measurements of an estuarine slurry ([30], experiment 15) with numerical simulation of the phenomenological model. The symbols represent the experimental data.

4. Application to continuous sedimentation

In their paper [8], Damasceno et al. simulated the behavior of a calcium carbonate slurry in an ICT. The corresponding constitutive functions $K(\phi)$ and $\sigma_e(\phi)$ had been determined in a similar way as by Tiller and Kwon [21] using γ-ray absorption measurements. Using the approaches (13) and (14), Damasceno et al. [35] obtained the constitutive equation $\sigma_e(\phi) = 0$ for $0 \le \phi_c = \phi_c^6 = 0.1$ and

$$\sigma_e(\phi) = \sigma_e^6(\phi) = 5.7\left[\left(\frac{\phi}{0.1}\right)^{9.09} - 1\right]\ \text{Pa}\quad \text{for}\ \phi > \phi_c^6.$$

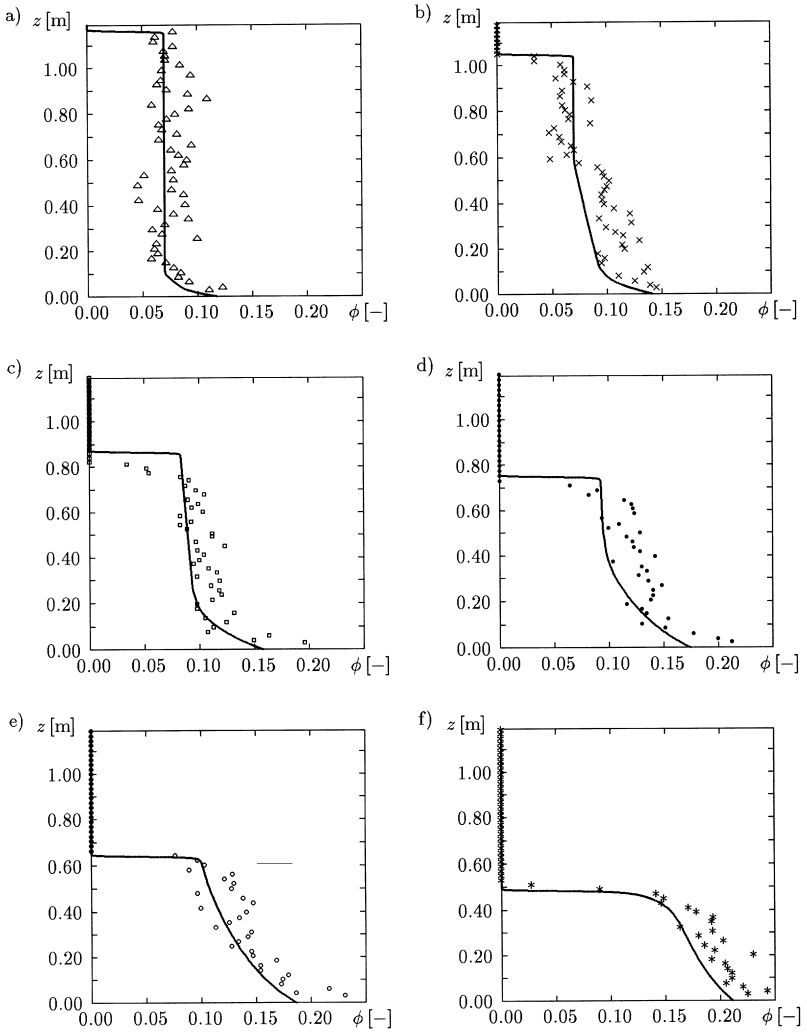

Fig. 9. Comparison of γ-ray concentration measurements of a kaolin suspension [34] with numerical simulation of the corresponding phenomenological sedimentation model. (a) $t = 0.052$ d; (b) $t = 0.312$ d; (c) $t = 0.87$ d; (d) $t = 2.13$ d; (e) $t = 3.91$ d; (f) $t = 13.27$ d.

The resulting permeability was

$$K(\phi) = 1.0 \times 10^{-10} \left(\frac{\phi}{0.1}\right)^{-9.47} \text{m}^2 = 3.388 \times 10^{-20} \phi^{-9.47} \text{m}^2,$$

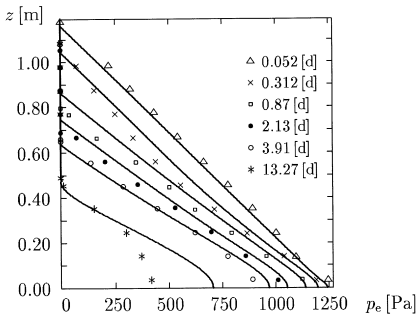

Fig. 10. Comparison of excess pore pressure measurements of a kaolin suspension [34] with numerical simulation of the phenomenological model. The times correspond to those of Fig. 9.

using concentration values varying between 0.18 and 0.25 ([8], Fig. 2). Applying formula (Eq. (16)) leads to

$$f_{\text{bk}}(\phi) = f_{\text{bk}}^6(\phi) = -5.517 \times 10^{-13} \phi^{-7.47} \text{ m/s} \quad \text{for } \phi > 0.18;$$

this expression was cut at $\phi = \phi_{\max} = 0.3$. The particular mathematical model proposed in [8] does not include the hindered settling zone, nor is original experimental information available from which the initial settling rate could be inferred. Therefore, we constructed the remaining part of $f_{\text{bk}}^6(\phi)$, for ϕ between 0 and 0.18, simply by choosing Michaels and Bolger's equation (Eq. (12)) with $\phi_{\max} = 0.3$ and determining the parameters u_∞ and C such that $f_{\text{bk}}(\phi)$ is differentiable at $\phi = 0.18$, leading to

$$f_{\text{bk}}^6(\phi) = -1.9802137 \times 10^{-4} \phi \left(1 - \frac{\phi}{0.3}\right)^{5.647} \text{ m/s} \quad \text{for } 0 \le \phi \le 0.18.$$

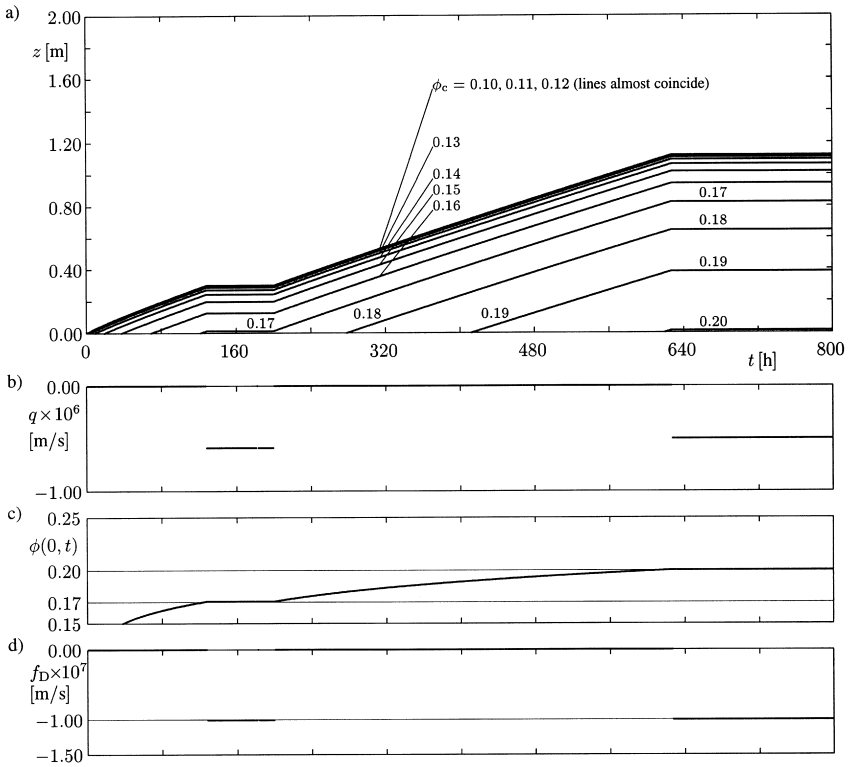

Fig. 11. Simulation of the filling up of an ICT and transition between steady states. (a) Settling plot showing the iso-concentration lines corresponding to the annotated values; (b) the prescribed values of $q(t)$ during the simulation; (c) the simulated discharge concentration $\phi(0, t)$, compared to the desired steady state values 0.17 and 0.20; (d) the simulated discharge solids volume flux $f_D(t) = q(t)\phi(0, t)$. Parameters are chosen according to Damasceno et al. [8], see Tables 2 and 3.

The functions $f_{bk}^6(\phi)$ and $\sigma_e^6(\phi)$ are drawn in Fig. 1e. The main differences of the mathematical model proposed in [8] compared with the phenomenological theory used in this paper, although both emerge from the theory of mixtures, consists of the neglection of the hindered settling zone and inclusion of advective acceleration terms, which we have neglected. Damasceno et al. [8] employed their mathematical model to simulate the filling up of a continuous thickener and the transition between steady states, and to compare several operation strategies.

We have adopted their parameters in the construction of our numerical example of filling up and changing of steady states of an ICT of feeding level height $L = 2\,\text{m}$ (see Fig. 11).

The two steady states considered here and the operating conditions assumed in our example are given in Tables 2 and 3; for details on steady states refer to [5,7,18].

It should be noted that our numerical result confirms the conclusion drawn by Damasceno et al. [8] that the filling up of an ICT at a given feed flux can be performed much

Table 2
Parameters adopted from Damasceno et al. [8], of the steady states considered in Table 3 and Fig. 11

i	$q = q^i$ (10^{-7} m/s)	ϕ_D^i	ϕ_L^i	f_F^i (10^{-7} m/s)	z_c (m)
1	−5.882	0.17	0.0005083305	−1.0	0.29
2	−5.0	0.20	0.000508561	−1.0	1.11

Table 3
Operating conditions, adopted from Damasceno et al. [8], for the simulation shown in Fig. 11[a]

Time interval	$q(t)$	$\phi_L(t)$	$f_F(t)$	Remarks
$t \le 0$				ICT is initially empty
$0 < t \le t*$	0.0	0.0005114092	-1.0×10^{-7} m/s	ICT is filled up until ϕ (0.005, t) attains $\phi_D^1 = 0.17$ at $t^* \approx 129\,\text{h}$
$t* < t \le 72\,\text{h}$	q^1	0.0005083305	-1.0×10^{-7} m/s	ICT operates near steady state 1
$72\,\text{h} < t \le t**$	0.0	0.0005111792	-1.0×10^{-7} m/s	Sediment level and $\phi(0, t)$ increase until $\phi(0.005, t)$ attains $\phi_D^2 = 0.20$ at $t^{**} \approx 626\,\text{h}$
$t > t**$	q^2	0.0005085611	-1.0×10^{-7} m/s	ICT operates near steady state 2

[a]The values $t*$ and $t**$ are obtained during the computation and are not given beforehand.

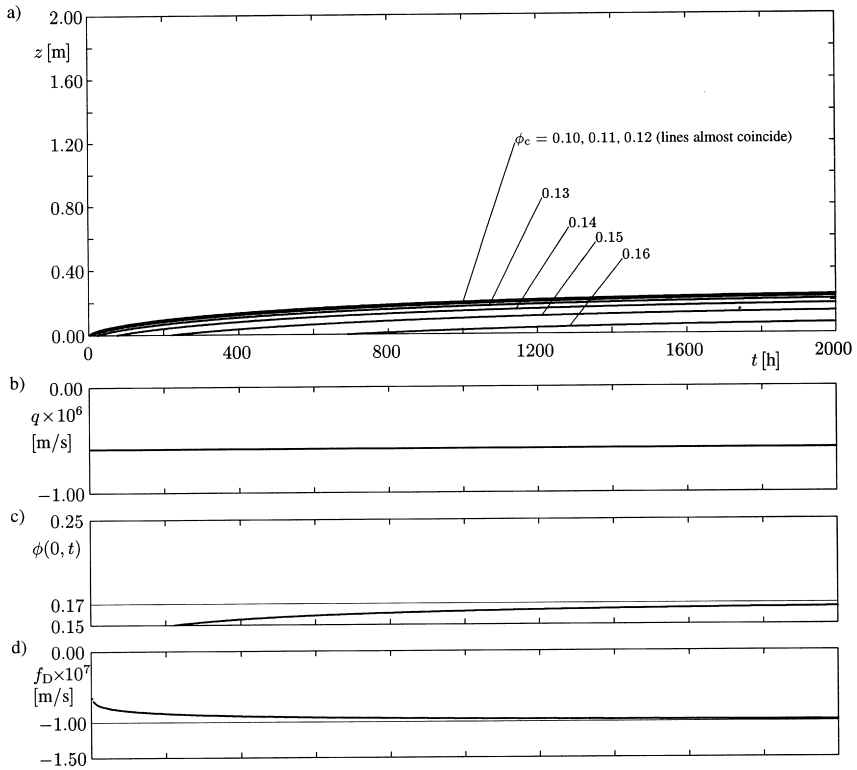

Fig. 12. Simulation of the filling up of an ICT keeping the volume average velocity and the feed flux constant. (a) Settling plot showing the iso-concentration lines corresponding to the annotated values; (b) the prescribed value of $q(t)$ during the simulation; (c) the simulated discharge concentration $\phi(0, t)$, compared with the desired steady state value 0.17; (d) the simulated discharge solids volume flux $f_D(t) = q(t)\phi(0, t)$. Parameters are chosen according to Damasceno et al. [8], see Tables 2 and 3.

more rapidly if the vessel is kept closed rather than left open, such that the volume average velocity takes desired steady state value; and that similarly, by closing the vessel during transition between steady states, the sediment level rises more quickly than if $q(t)$ is changed directly between steady state values. The first of these statements is illustrated by Fig. 12; we started from a thickener full of water as in Fig. 11 and kept $q(t)$ and $\phi_L(t)$ at the constant respective values q^1 and ϕ_L^1 during the whole simulation.

It was observed that the sediment built up very slowly, and even after 2000 h, nearly 3 months, it has not yet reached the desired steady state.

5. Conclusions

We now discuss the numerical results. Figs. 3 and 4 show qualitative agreement of the numerical simulation with the experimental concentration profiles. However, the phenomenological model predicts a distinctive clear liquid-suspension interface, while the concentration profiles measured at $t = 1800$ and 3000 s plotted in Fig. 3 indicate that the supernatant liquid above the bulk suspension is not entirely clear; there is a small amount of particles performing Brownian motion. This effect seems to be absent in the measurements given in Fig. 4. This figure also demonstrates that the mathematical model correctly predicts the transition of the concentration profiles from concave to convex shape and that the maximum concentration (for that experiment) of about 0.35 is predicted accurately. The quality of accordance visible in Fig. 4 is certainly due to the great accuracy of the measurements by which the constitutive functions were determined (see [27]).

It seems more difficult to apply the phenomenological theory of sedimentation, which is based on many idealizing assumptions, to natural slurries such as the material used by Been and Sills [30]; the experimental data permitted only very rough estimates of the functions $f_{bk}(\phi)$ and or $\sigma_e(\phi)$. Nevertheless, we found that the shapes of the concentration profiles calculated numerically approximated the shapes of the measured ones remarkably well, as can be seen in Figs. 5 and 7, and that the approximation of the excess pore pressure data measured in Been and Sills' experiment 15 was also satisfactory (see Fig. 8). Certainly additional efforts in determining the constitutive functions more accurately will still increase the accordance. Fig. 6 indicates that the simulated dissipation of excess pore pressure is much slower than the dissipation observed in the experiment. We conjecture that this is due to the formation of vertical channels such as those photographed by Glasrud et al. [36], through which the liquid flows upwards at an increased rate compared with its flow through the interstices of the sediment

layer. The rapid dissipation of excess pore pressure could also be due to the plastic deformation of the sediment bed at high loads, i.e. near the bottom of relatively large columns. The latter effect is also visible in Fig. 5 in the high measured concentration values near the bottom of the vessel. Inhomogeneities such as vertical channels, inherent to natural slurries, are not within the scope of the restriction of the phenomenological model to one space dimension, and will probably require a multidimensional treatment, while the high concentrations near the bottom of the vessel suggest that the phenomenological theory could still be improved by allowing an elasto-plastic deformation of the sediment.

Severe inhomogeneities also seem to have influenced Dreher's experimental configuration as expressed by the scattering of his measured concentration data [34], which are plotted in Fig. 9. Consequently, the simulated (smooth) profiles only roughly approximate his concentration measurements in the compression zone. However, the simulated propagation velocity of the sediment level agrees with the experimental observation. We note that the inclined straight sections of the simulated concentration profiles in Fig. 9b and c represent rarefaction waves, and are due to the simple modeling of f_{bk} by second-order polynomials. Again, as shown in Fig. 10, the simulated excess pore pressure values corresponding to Dreher's experiment near the bottom of the vessel, and for large times, are much higher than the measured values. The interpretation of this discrepancy is probably the same as for Been and Sills' experiment 11.

The experimental information available in the last study considered, the paper by Damasceno et al. [8], are plots of the data from which the effective solid stress and permeability functions were determined (their Figs. 1 and 2). Moreover, it is not evident to which feeding level height their simulations of discharge concentration and sediment height apply. However, the simulations presented in Figs. 11 and 12 agree qualitatively with their results, and show that constitutive functions obtained from batch tests can be employed successfully to simulate continuous thickening by the phenomenological model.

We found that all examples presented confirmed that the phenomenological theory is sound and predicted correctly the sedimentation–consolidation behavior of many flocculated suspensions, whose variety was expressed by the ranges of parameters presented in Table 1 and Fig. 1. At the same time, however, it seems desirable to have more additional experimental data available. The determination of f_{bk} in the hindered settling zone was performed here only very vaguely, and should for a rigorous treatment be based on a series of batch settling tests of dilute suspensions at sub-critical initial concentrations.

The available number of experimental studies of batch sedimentation is quite large, and it would certainly be interesting to consider the results by Blake and Colombera [37], Comings [38], Dell and Keleghan [39], Font [40], Font et al. [41], França et al. [42], Free [43], Gaudin and Fuerstenau [33], Kearsey and Gill [44], Scott [45,46], Shirato et al. [47] and Work and Kohler [48], which are not included here, as additional test cases for an extension of this study, although the older works present experimental batch settling results without suggesting equations that could describe the observed behavior. The phenomenological model will also be applied to experiments currently being performed by Garrido [49] under the second author's guidance.

In contrast to this vast body of knowledge, only few papers presenting experimental results of the behavior of flocculated suspensions under semi-batch or continuous flow conditions (Eklund and Jernqvist [50], Font and Laveda [51]) have been published. This is certainly due to the fact that continuous sedimentation experiments are much more difficult to perform than batch tests.

Acknowledgements

The preparation of this paper and its presentation at the conference were made possible through support by the United Engineering Foundation, by Fondef project DI97-12042 at the University of Concepción, and by the Sonderforschungsbereich 404 at the University of Stuttgart.

References

[1] H.G. Nichols, Trans. Inst. Min. Met. 17 (1908) 293.
[2] R.T. Mishler, Eng. Min. J. 94 (1912) 643.
[3] K.S. Coe, G.H. Clevenger, Trans. AIME 55 (1916) 356.
[4] R. Bürger, Chem. Eng. J. 80 (2000) 177–188.
[5] R. Bürger, M.C. Bustos, F. Concha, Int. J. Miner. Process. 55 (1999) 267.
[6] R. Bürger, F. Concha, in: H. Hoberg, H.V. Blottnitz (Eds.), Proceedings of the 20th International Mineral Process Congress, vol. 4, Aachen, Germany, 21–26 September 1997, GDNIB, Clausthal-Zellerfeld, 1997, p. 91.
[7] R. Bürger, F. Concha, Int. J. Multiphase Flow 24 (1998) 1005.
[8] J.J.R. Damasceno, H.M. Henrique, G. Massarani, in: Proceedings of the Third Meeting of the Southern Hemisphere on Mineral Technology, São Lourenço, Minas Gerais, Brazil, 1992, p. 675.
[9] S. Whitaker, Transp. Porous Media 1 (1986) 3.
[10] K.A. Landman, L.R. White, Adv. Colloid Interf. Sci. 51 (1994) 175.
[11] R. Bürger, W.L. Wendland, F. Concha, Z. Angew. Math. Mech. 80 (2000) 79.
[12] F. Concha, M.C. Bustos, A. Barrientos, E. Tory (Eds.), Sedimentation of Small Particles in a Viscous Fluid (1996) Computational Mechanics PublicationsSouthampton.
[13] M.C. Bustos, F. Concha, R. Bürger, E.M. Tory, Sedimentation and Thickening (1999) Kluwer Academic PublishersDordrecht, The Netherlands.
[14] R. Bürger, W.L. Wendland, Math. Methods Appl. Sci. 21 (1998) 865.
[15] G.J. Kynch, Trans. Faraday Soc. 48 (1952) 166.
[16] A.S. Michaels, J.C. Bolger, Ind. Eng. Chem. Fund. 1 (1962) 24.
[17] J.E. Richardson, W.N. Zaki, Trans. Inst. Chem. Eng. (London) 32 (1954) 35.
[18] R. Bürger, S. Evje, K.H. Karlsen, K.-A. Lie, Chem. Eng. J. 80 (2000) 91–104.
[19] M.C. Bustos, F. Concha, W.L. Wendland, Math. Methods Appl. Sci. 13 (1990) 1.
[20] P.T. Shannon, E.M. Tory, SME Trans. 235 (1966) 375.
[21] F.M. Tiller, private communication, December 1997.

[22] F.M. Tiller, N.B. Hsyung, Y.L. Shen, Proceedings of the Fifth World Congress on Filtration 2 (1991) 80Soc. Française de FiltrationNice, France.
[23] F.M. Tiller, W. Leu, J. Chin. Inst. Chem. Eng. 11 (1980) 61.
[24] F.M. Tiller, W. Chen, Chem. Eng. Sci. 43 (1988) 1695.
[25] F.M. Tiller, AIChE J. 27 (1981) 823.
[26] R. Bürger, W.L. Wendland, F. Concha, in: K.P. Holz, W. Bechteler, S.S.Y. Wang, M. Kawahara (Eds.), Proceedings of the Third International Conference on Hydro-Science and Engineering, Cottbus/Berlin, Germany, August 31–September 3, 1998, The University of Mississippi, Carrier Hall, MS, USA, 1998, p. 222 (abstract, full length paper published on CD-ROM).
[27] L. Bergström, J. Chem. Soc. Faraday Trans. 88 (1992) 3201.
[28] F.M. Auzerais, R. Jackson, W.B. Russel, J. Fluid Mech. 195 (1988) 437.
[29] H.C. Brinkman, Appl. Sci. Res. A1 (1947) 27.
[30] K. Been, G.C. Sills, Géotechnique 31 (1981) 519.
[31] R. Becker, Engineering thesis, Department of Metallurgical Engineering, University of Concepción, 1982.
[32] R. Bürger, F. Concha, K.-K. Fjelde, K.H. Karlsen, Powder Technol., in press.
[33] A.M. Gaudin, M.C. Fuerstenau, Trans. AIME 223 (1962) 122.
[34] T. Dreher, Preprint 97/34, Sonderforschungsbereich 404, University of Stuttgart, 1997.
[35] J.J.R. Damasceno, R. Souza, G. Massarani, in: Proceedings of the XIX Encontro sobre Escoamento em Meios Porosos, Campinas, São Paulo, Brazil, 1991.
[36] G.G. Glasrud, R.C. Navarrete, L.E. Scriven, C.W. Macosko, AIChE J. 39 (1993) 560.
[37] J.R. Blake, P.M. Colombera, Chem. Eng. Sci. 32 (1977) 221.
[38] E.W. Comings, Ind. Eng. Chem. 32 (1940) 663.
[39] C.C. Dell, W.T.H. Keleghan, Powder Technol. 7 (1973) 189.
[40] R. Font, Chem. Eng. Sci. 46 (1991) 2473.
[41] R. Font, P. García, M. Pérez, Sep. Sci. Technol. 33 (1998) 1487.
[42] S.C.A. França, G. Massarani, E.C. Biscaia Jr., Powder Technol. 101 (1999) 157.
[43] E.E. Free, Eng. Min. J. 101 (1916) 681.
[44] H.A. Kearsey, L.E. Gill, Trans. Inst. Chem. Eng. 41 (1963) 296.
[45] K.J. Scott, Trans. Inst. Min. Met. 77 (1968) C85.
[46] K.J. Scott, Ind. Eng. Chem. Fund. 9 (1970) 422.
[47] M. Shirato, H. Kato, K. Kobayashi, H. Sakazaki, J. Chem. Eng. Jpn. 3 (1970) 98.
[48] L.T. Work, A.S. Kohler, Ind. Eng. Chem. 32 (1940) 1329.
[49] P. Garrido, Determinación de parámetros de sedimentación mediante atenuación de rayos X, Doctoral thesis, Department of Metallurgical Engineering, University of Concepción, in preparation.
[50] L.G. Eklund, Å. Jernqvist, Chem. Eng. Sci. 30 (1975) 597.
[51] R. Font, M.L. Laveda, Chem. Eng. Sci. 51 (1996) 5007.